Diffusion and Perfusion Magnetic Resonance Imaging, edited by D. Le Bihan.
Raven Press, Ltd., New York © 1995.

CHAPTER 18

Functional MR Imaging Using the BOLD Approach

Dynamic Characteristics and Data Analysis Methods

Peter A. Bandettini, Eric C. Wong, Jeffrey R. Binder, Stephen M. Rao, A. Jesmanowicz, Elizabeth A. Aaron, Timothy F. Lowry, Hubert V. Forster, R. Scott Hinks, and James S. Hyde

In the past two years, magnetic resonance imaging (MRI) has demonstrated the capability of detecting increases in cerebral blood volume (1), flow (2), and oxygenation (2–5), that locally occur in association with increased neuronal activity.

The most widely used MRI method for the noninvasive mapping of human brain activity is based on blood oxygenation level dependent (BOLD) contrast (6). Local cerebral blood oxygenation is understood to increase with neuronal activity (7–10). A small but significant local signal increase in activated cortical regions is observed with the use of T_2^*- or T_2-weighted pulse sequences. A working model of this phenomenon is that an increase in neuronal activity causes local vasodilatation which, in turn, causes blood flow to increase in such a manner that the amount of paramagnetic deoxyhemoglobin in the local vasculature is reduced. The reduction in deoxyhemoglobin causes an increase in spin coherence (increase in T_2 and T_2^*).

Several studies have provided support for this model. Cerebral blood oxygenation changes have been shown to modulate brain tissue T_2 and T_2^* (6,11–15). The amount of signal enhancement in activated cortical regions has been shown to be field-strength (4,16–18) and echo-time (4,17,19,20) dependent. In addition, greater activation-induced spin-spin relaxation rate changes are observed with gradient-echo than with spin-echo sequences at a given echo time (19,21–24). Mathematical simulations based on simplified models of the cerebral vasculature (25–28) are in agreement with MRI observations.

Observations have been made regarding the response characteristics of the BOLD signal enhancement with neuronal activation. The latency of the activation-induced BOLD signal change in primary cortical regions is approximately 5 to 8 seconds from stimulus onset to 90% maximum, and is 5 to 9 seconds from stimulus cessation to 10% above baseline (2,29,30). In some studies, regions hypothesized to be involved with higher cognitive function have demonstrated longer activation latencies (31). Occasional observations that are less understood include an undershoot in signal after activation (2), and a decrease in the baseline value after the first activation period during cyclic activation (5). A *decrease* in the signal during activation is occasionally observed in some cortical regions (32). During photic stimulation, signal oscillations in the activated regions have been reported which, in neighboring pixels, have the same frequency but are shifted in time (32). It is not understood whether these oscillations are neuronal or vascular in origin.

P. A. Bandettini, E. C. Wong, A. Jesmanowicz, and J. S. Hyde: Biophysics Research Institute, Medical College of Wisconsin, Milwaukee, Wisconsin 53226.

S. M. Rao and J. R. Binder: Department of Neurology, Medical College of Wisconsin, Milwaukee, Wisconsin 53226.

E. A. Aaron, T. F. Lowry, and H. V. Forster: Department of Physiology, Medical College of Wisconsin, Milwaukee, Wisconsin 53226.

R. S. Hinks: Applied Science Laboratory, G.E. Medical Systems, Milwaukee, Wisconsin 53201.

Visual cortex activation studies have shown that BOLD signal enhancement has essentially the same flicker frequency dependency (2) as that of cerebral blood flow changes observed using positron emission tomography (PET) (33).

The change in blood oxygenation that occurs upon brain activation is relatively slow and may be more extensive (i.e., large draining veins) than the actual activated regions (20,21,24,34,35). In addition, at extremely short repetition times in conjunction with large flip angles, activation-induced signal changes in gradient-echo sequences may partly be due to flow changes (i.e., apparent T_1 changes) (34). In general, because the number of variables that may contribute to the activation-induced signal change is large, it is difficult to correlate the magnitude and location of the signal change with the degree, extent, and distribution of neuronal activation.

Questions that need to be addressed in regard to BOLD contrast as it relates to magnetic resonance functional neuroimaging fall into four general categories: (i) the upper limits of *functional* temporal resolution, (ii) the upper limits of *functional* spatial resolution, (iii) correlation of the induced signal enhancement magnitude with underlying neuronal activity, and (iv) other significant physiological information that may be contained in the signal. The answers depend largely upon the temporal and spatial characteristics of the vascular response to neuronal activation in addition to the relationship between the MRI signal enhancement and details concerning vessel geometry and the pixel by pixel distribution of blood oxygenation, volume, and velocity. In addition, the temporal and spatial nature of intrinsic background fluctuations of signal, unrelated to activation-induced signal enhancement, need to be characterized.

In this group of studies, echo-planar imaging (EPI) (36) was used to obtain time courses of T_2^*-weighted images. To obtain information about the dynamics of the activation-induced signal changes, the subjects were given primary sensory stimuli and motor activation tasks that are varied in duration, timing, and rate. In addition, activation-induced and resting brain signal changes were observed during hypercapnic and hypoxic states. Post-processing methods are described which use oscillating on-off brain activation time course series to (i) create brain activation images which have reduced artifactual contamination (37) and (ii) extract spatially distributed activation phase information (38).

METHODS

We perform single-shot 64 × 64 resolution EPI on a standard clinical 1.5 Tesla GE Signa scanner with an inserted three-axis balanced torque head gradient coil designed for rapid gradient switching (39). A shielded quadrature elliptical endcapped transmit/receive birdcage rf coil (40) is used to obtain high quality images throughout the entire brain volume. Typically, single or multislice time course series of 64 to 1,024 susceptibility weighted (TE = 40 ms) gradient-echo images are obtained with a TR of 0.1 to 6 seconds, FOV of 24 cm, and slice thickness of 10 mm.

DYNAMIC STUDIES

Duration Effects

To observe the effects of both short term and long term activation of the primary motor cortex, subjects were instructed to tap their fingers to thumb in a self paced, consistent, and repetitive manner for durations ranging from 0.5 s to 6 minutes. The impulse response and steady-state characteristics of the induced vascular response were thereby obtained.

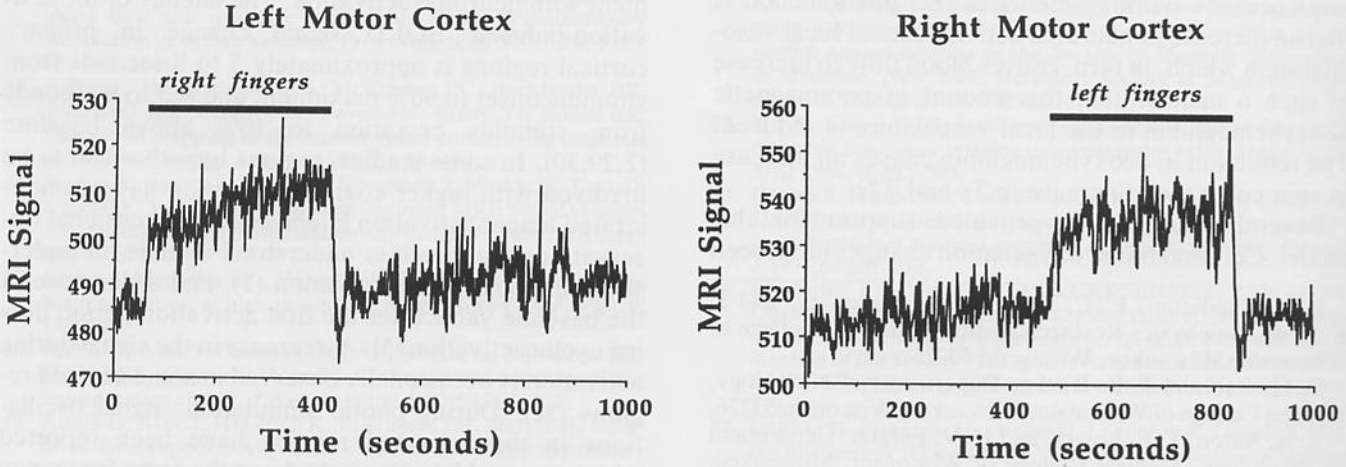

FIG. 1. Time-course plots (16:40 in duration) from pixels in the left and right motor cortices (TE/TR = 40 ms/1,000 ms). The subject performed self-paced sequential tapping of the fingers to thumb on the right then left hand for 6 minutes each.

In one study, the subject performed the finger tapping task first on the right hand for 6 minutes, then on the left hand for 6 minutes (TR = 1 s). The time courses from the left and right motor cortices, shown in Fig. 1, demonstrate that the signal from the primary motor cortex remained elevated and relatively stable even for these extremely prolonged durations of finger movement. In addition the study was repeated with a TR of 6 seconds to allow complete magnetization recovery between sequential images, thus eliminating any T_1 or inflow sensitization. The results again showed a consistent elevation of signal during the entire duration of activation, giving evidence that oxygenation, and not just flow, remains in an elevated state for the entire 6 minutes of activation.

In another study, subjects were cued twice during a time course to perform bilateral tapping of the forefinger to thumb, at maximal tapping frequency (≈6 Hz), for periods of time from 0.5 to 5 s (TR = 1 s). Figure 2 shows the signal from the same pixel in the motor cortex for each of the time courses. For the 0.5 s activation duration, signal enhancement began 2 to 3 s after the onset of activation and continued for another 3 to 5 seconds before returning to baseline. For all activation durations, the signal returned to baseline approximately 8 seconds after the cessation of movement.

The cerebral vascular transit time is approximately 3 seconds and the capillary transit time is approximately 1 second. Because the latency of the MR response is significantly longer, it is clear that the transit time is not the dominant source of the latency. It is well known that temporal and spatial summation in the nervous system occurs and can create time constants which are long compared to the time scale of neuronal firing. It may be that the large population of vascular sphincters which locally control blood flow rate have different opening thresholds, thus creating a graded increase in blood flow in response to the temporal pattern of neuronal activation.

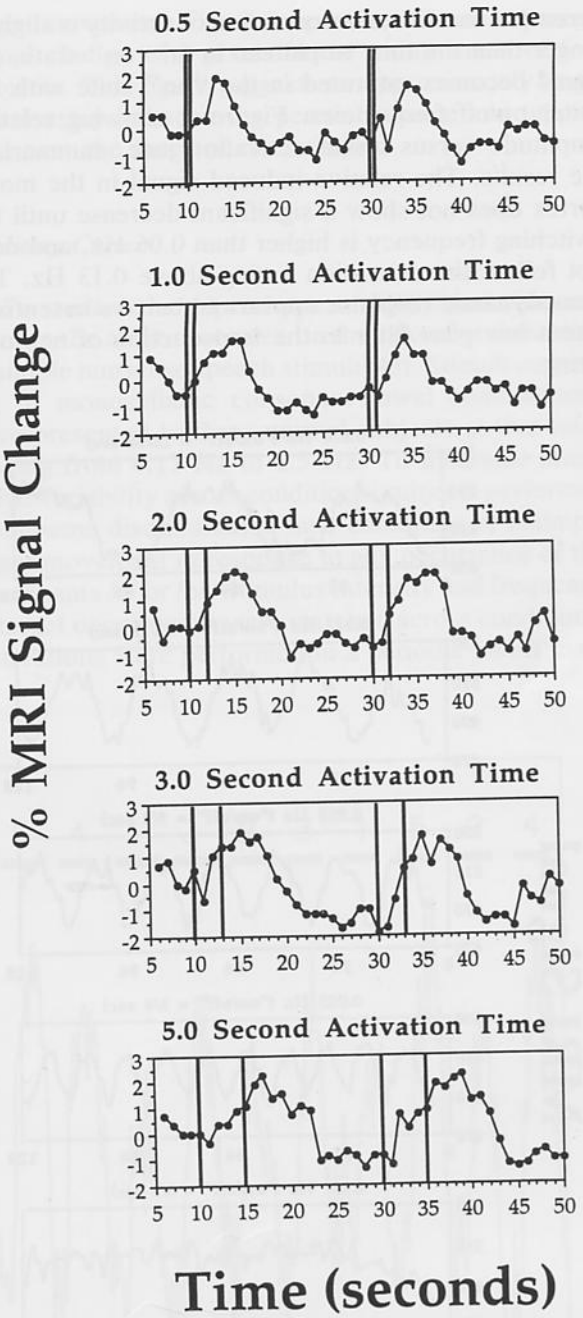

FIG. 2. Time courses from the same pixel in the motor cortex (TE/TR = 40 ms/1,000 ms) obtained during two episodes of finger tapping (≈6 Hz) for durations ranging from 0.5 s to 5 s.

On/Off Switching Rate Effects

The following on/off (i.e., active/resting) switching rate study was motivated, in part, by the desire to maximize both the induced signal amplitude and the number of activation cycles in a time course. These goals are important so that high quality brain activation images can be created by temporal cross-correlation or Fourier analysis, and relative spatially-distributed latency can be extracted by cross-correlation of a shifting reference function with the time course of each pixel (37). Also, this analysis determines the on/off rate-dependent damping of the activation induced signal enhancement by the intrinsic hemodynamic response time.

To test the dependence of signal amplitude on the on/off switching frequency, subjects tapped their fingers to thumb, bilaterally, in a self-paced, consistent, and repetitive manner for on/off cycles ranging from 0.02 Hz (25 seconds "on" and 25 seconds "off") to 0.5 Hz (1 seconds "on" and 1 seconds "off") in frequency (TR = 1 s). Figure 3 shows the time courses from the same pixel for on/off finger activation frequencies ranging from 0.02 Hz to 0.5 Hz. Because the time

to reach a baseline after cessation of activity is slightly longer than the time to plateau in an "on" state, the signal becomes saturated in the "on" state with the faster on/off frequencies. Figure 4, showing relative amplitude versus on/off activation rate, summarizes the results. The relative induced signal in the motor cortex does not show a significant decrease until the switching frequency is higher than 0.06 Hz, and does not follow the activation timing above 0.13 Hz. The hemodynamic response appears to behave essentially like a low pass filter in the transduction of neuronal firing.

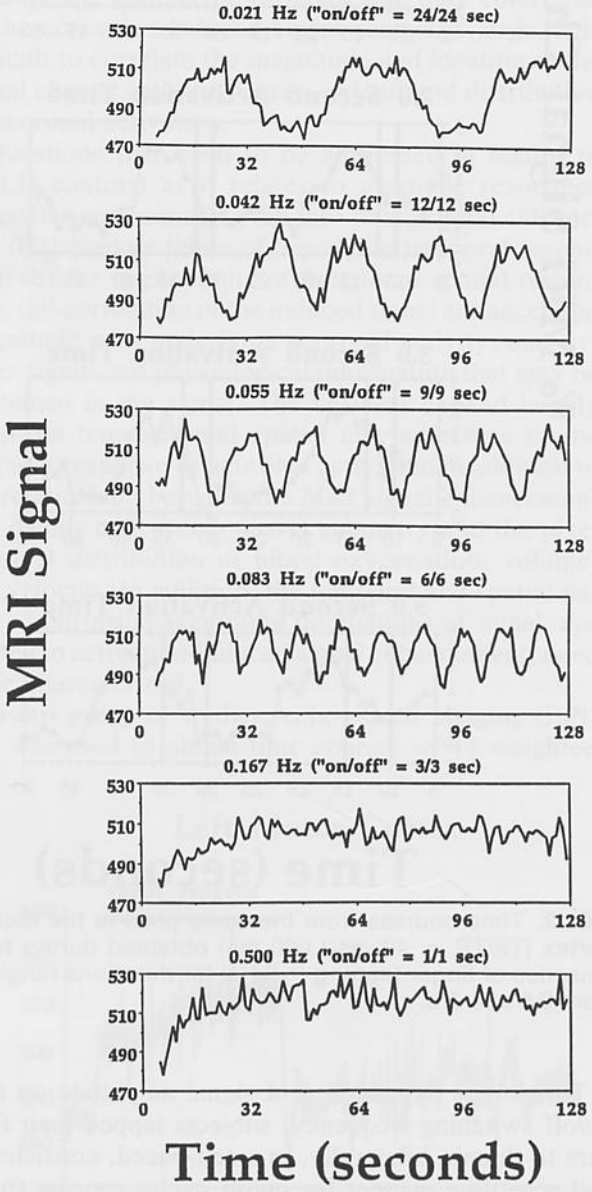

FIG. 3. Time courses from the same pixel in the motor cortex (TE/TR = 40 ms/1,000 ms) obtained during cyclic on/off finger movement. As the on/off frequency is increased from 0.024 Hz to 0.5 Hz, the activation-induced amplitude becomes decreased, and the overall signal becomes saturated in the "on" state.

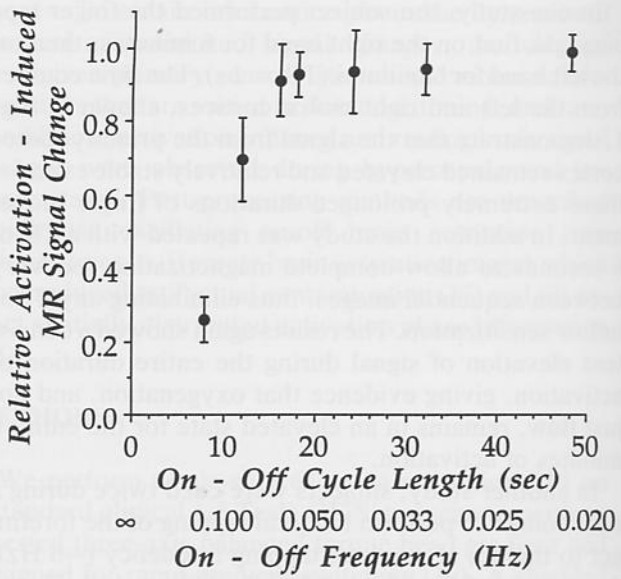

FIG. 4. Summary of the dependence of the relative amplitudes of the activation-induced signal on the switching frequency. The activation-induced signal begins to become diminished above the on/off rate of 0.016 Hz (8 seconds "on" and 8 seconds "off").

Effects of Finger Tapping and Syllable Presentation Rate

In addition to temporal aspects of the activation procedure, the magnitude of the event-related signal changes observed using BOLD contrast may depend upon physical characteristics of the stimulus input. Like PET, the observed BOLD signal changes presumably reflect metabolic activity integrated over time within a large neuronal pool. If each presentation of a stimulus results in a similar set of neuronal events, then the integrated neuronal response, and possibly the resulting blood flow response, will be a linear function of the number of stimuli presented per unit time (31). Regional cerebral blood flow in the visual cortex was shown in one PET study to have a positive, linear dependence on the rate of stimulation up to approximately 8 Hz (41). An identical rate-response function has been demonstrated in the visual cortex using neuro-functional MRI techniques (2). Effects of auditory word presentation rate have been demonstrated in some but not all active areas of the temporal lobe auditory cortex using PET (42).

In the following studies, the activation induced BOLD signal enhancement is observed in the motor and auditory cortices relative to syllable presentation and finger flexion rate respectively.

Motor Cortex

Four right-handed healthy subjects performed flexion-extension movements of the fingers of the right

hand (digits 2–5 in unison) in response to a metronome presented over a pneumatic audio system. The metronome produced clicking sounds at rates of 1, 2, 3, 4, or 5 Hz. Two axial slices (8 mm slice thickness) were selected to include the hand region of the primary motor cortex. Imaging consisted of three consecutive 480-sec scanning series (TR = 1 s). During a given series, movements were performed for 12 s followed by 12 s of rest, with a total of 20 consecutive on/off cycles per series. The 20 cycles consisted of four repetitions of the five movement rates, presented in a pseudorandom order. In all, each of the five movement rates was replicated 12 times (four repetitions per series, three series).

Figure 5 shows the time course from a pixel selected in the motor cortex of one subject during episodes in which the tapping rate was varied. The dark lines indicate the time period during the activation-induced signal enhancement. The numbers above these lines indicate the metronome rates. Note that the degree of signal change is consistently proportional to the rate of finger movement. Figure 6 represents the mean percent signal change of 3 pixels in the motor areas of four subjects. This figure suggests an approximately linear relationship between the percent change and tapping rate over the range of rates studied.

Auditory Cortex

We studied the dependence of MR signal enhancement in the auditory cortex on the rate of presentation of simple nonsense speech stimuli (43). Stimuli consisting of monosyllabic consonant-vowel combinations were presented to three normal subjects at five rates ranging from 0.17 Hz to 2.5 Hz. To minimize attentional variability across conditions, subjects performed a phoneme discrimination task consisting of a simple finger movement in response to any occurrence of the consonants /d/ or /b/. Stimulus intensity and frequency of target occurrences were matched across conditions. Activations were performed in a periodic on/off man-

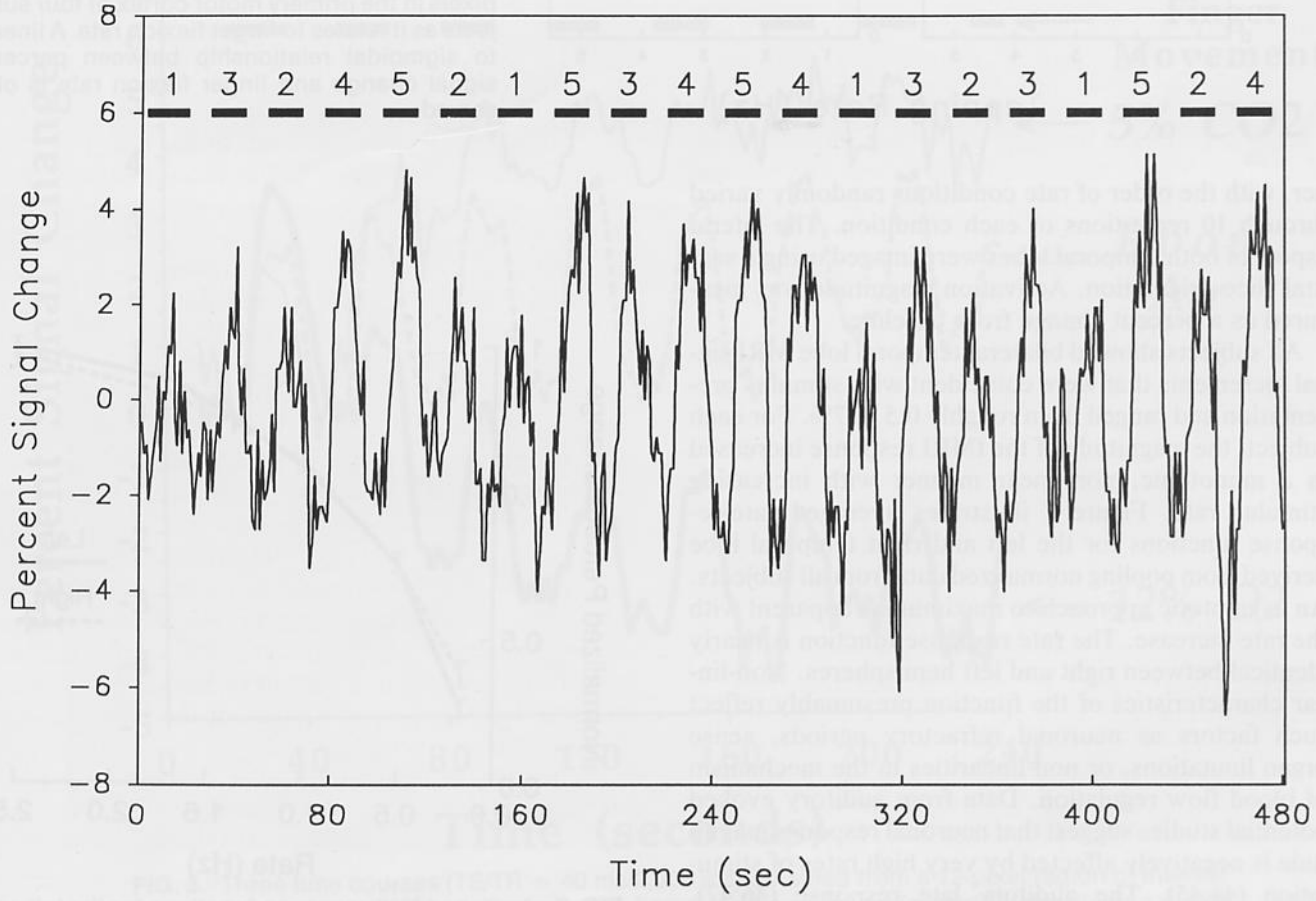

FIG. 5. Time courses from a pixel in the primary motor cortex (TE/TR = 40 ms/1,000 ms) during 20 episodes (20 seconds "on," 20 seconds "off") of finger flexion. The frequency of finger flexion was varied in rate between 1 and 5 Hz per episode, indicated by the numbers above the bars indicating when the signal enhancement took place. Note that the amplitude of the signal change demonstrates a dependence upon the finger flexion rates.

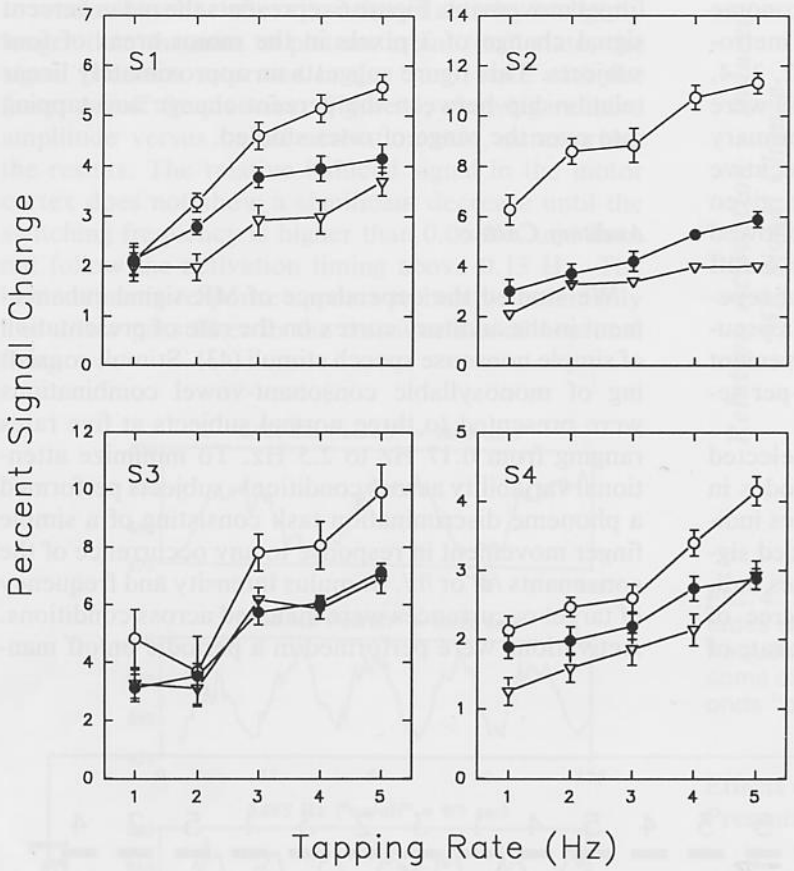

FIG. 6. The percent signal change from three pixels in the primary motor cortex of four subjects as it relates to finger flexion rate. A linear to sigmoidal relationship between percent signal change and finger flexion rate is observed.

ner, with the order of rate conditions randomly varied through 10 repetitions of each condition. The lateral aspect of both temporal lobes were imaged using a sagittal slice orientation. Activation magnitude was measured as a percent change from baseline.

All subjects showed bilateral temporal lobe MRI signal increments that were coincident with stimulus presentation and ranged from roughly 0.5 to 7%. For each subject, the magnitude of the fMRI response increased in a monotonic, non-linear manner with increasing stimulus rate. Figure 7 illustrates averaged rate-response functions for the left and right temporal lobe derived from pooling normalized data from all subjects. An asymptotic approach to maximum is apparent with the rate increase. The rate response function is nearly identical between right and left hemispheres. Non-linear characteristics of the function presumably reflect such factors as neuronal refractory periods, sense organ limitations, or non-linearities in the mechanism of blood flow regulation. Data from auditory evoked potential studies suggest that neuronal response magnitude is negatively affected by very high rates of stimulation (44,45). The auditory late response (46,47), which may have a neural substrate similar to that of the temporal lobe responses observed in the study, has been shown to decrease exponentially with increasing stimulus rate (48,49). This negative effect, added to the

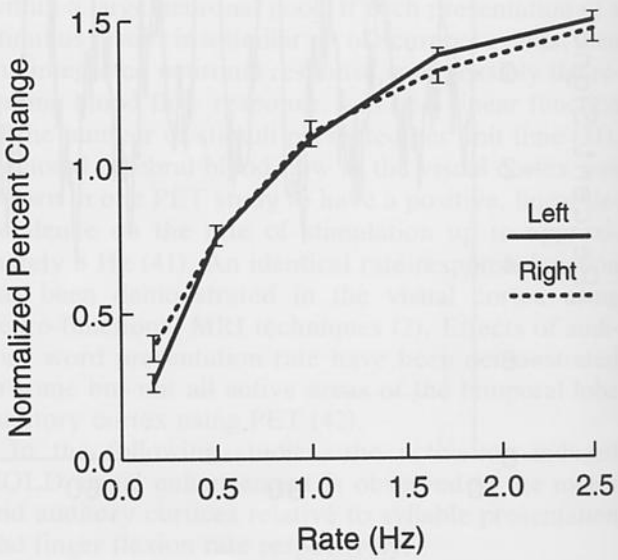

FIG. 7. Averaged rate-response functions for the left and right temporal lobe derived from pooling normalized data from three subjects. Stimuli were monosyllabic consonant-vowel combinations presented at rates from 0.17 to 2.5 Hz.

positive integrative effect of the increasing rate, would produce an exponential decay and eventual downward turn of the rate-response function with higher rates. Our data are in good agreement with the first of these expectations, and a downward turn has been documented in the visual system at very fast flicker rates (2,33). In contrast to one PET study (42), we observed no auditory areas that were free of rate effects. This could have resulted from a failure to include such areas in the slice selection, from the "nonsense" nature of the consonant-vowel stimuli, or from other unknown factors.

Effects of Hypoxia and Hypercapnia

The effects of alterations in the concentration of oxygen and carbon dioxide in inhaled air on the amplitude of the activation-induced signal change in humans has not previously been tested. In this study, a volunteer breathed, during three separate time courses: (i) room air, (ii) air containing 5% CO_2, and (iii) air containing 12% oxygen (TR = 2 s). The time course length was 240 seconds. The subject began breathing altered air after a 30 second baseline and resumed breathing room air at 210 seconds.

In one study, cyclic, bilateral, self-paced tapping of fingers to thumbs was performed during the three time courses. In another study during the same imaging session, the three time courses were performed in the absence of finger tapping so that the spatially variant changes that occur with hypercapnia and hypoxia could be discerned.

Three time courses in the identical 12-pixel region in the motor cortex, shown in Figure 8, demonstrate sensitivity of the overall and activation-induced signal

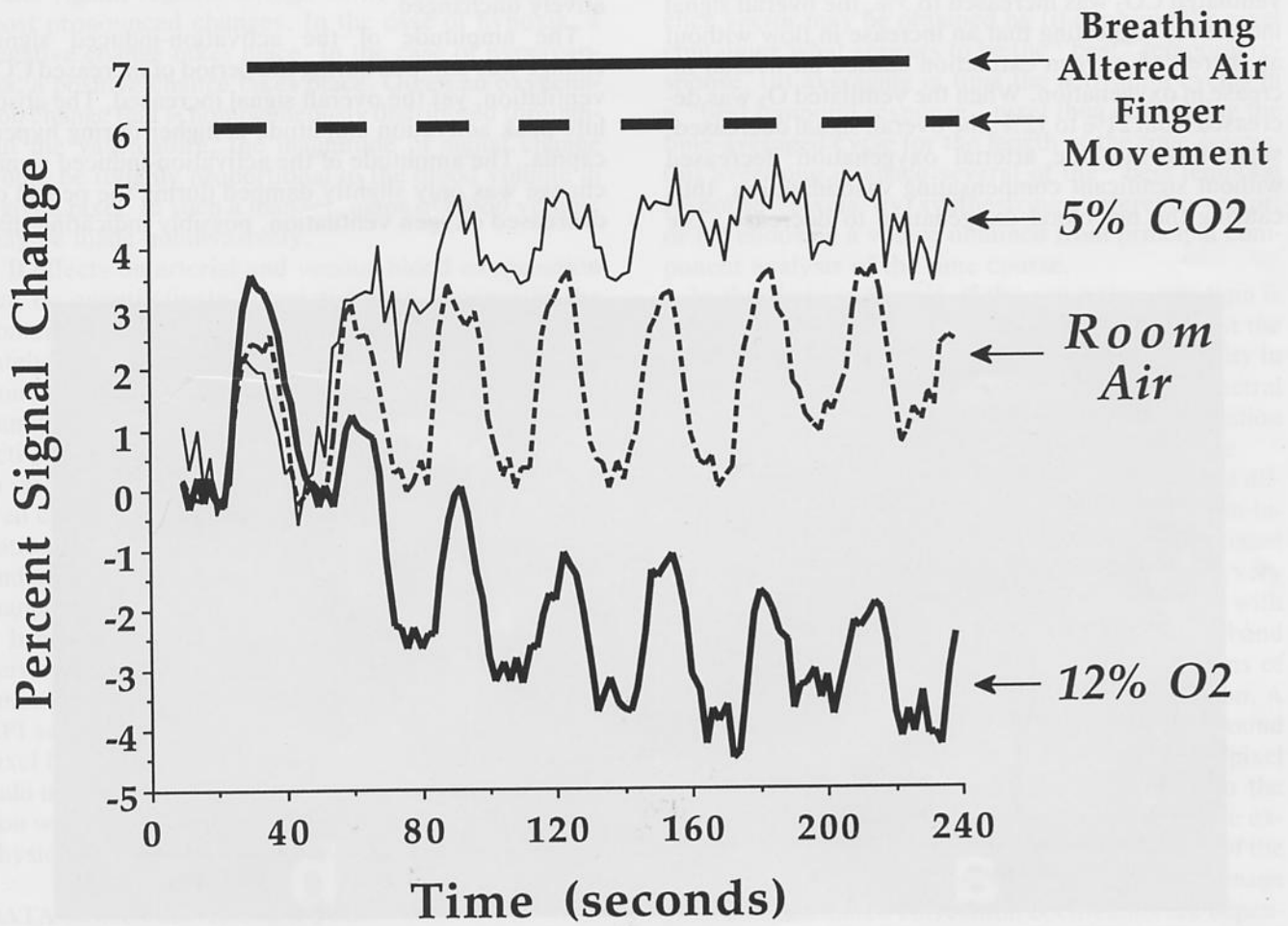

FIG. 8. Three time courses (TE/TR = 40 ms/2,000 ms) obtained from a 12-pixel region of interest in the motor cortex. Self-paced sequential finger tapping was performed bilaterally in a cyclic on/off manner, during which the subject breathed, in separate time courses, room air, air with 5% CO_2, and air with 12% O_2 for 3 minutes (after an initial baseline period of 30 seconds). With increased CO_2, overall signal is increased and activation-induced signal change is strongly damped. With decreased O_2 (from 21% in room air), overall signal is decreased, but the activation-induced signal changes is only slightly damped.

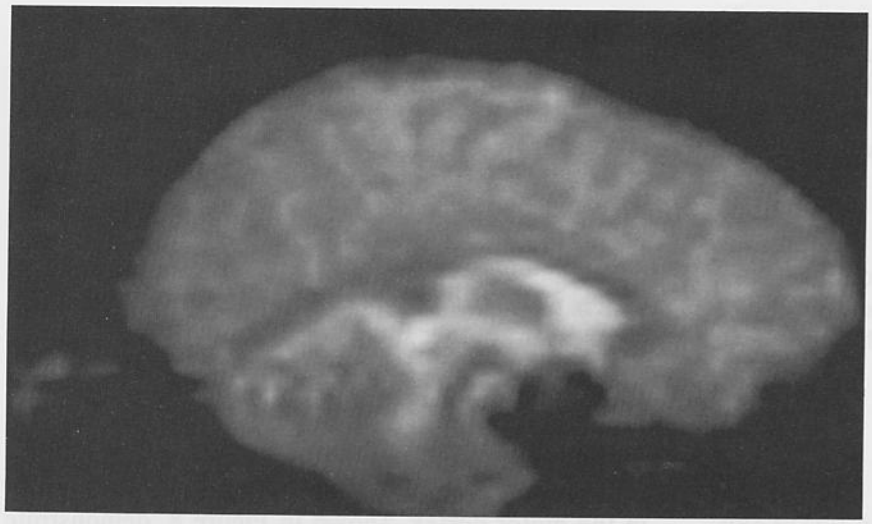

FIG. 9. Gradient-echo echo-planar image (TE/TR = 40 ms/∞) of the slice observed duration hypoxia and hypercapnic states.

change to hypoxic and hypercapnic states. When the ventilated CO_2 was increased to 5%, the overall signal increased, suggesting that an increase in flow without an increased oxygen extraction caused an overall increase in oxygenation. When the ventilated O_2 was decreased from 21% to 12%, the overall signal decreased, suggesting that the arterial oxygenation decreased without significant compensating vasodilatation, thus causing the net blood oxygenation to decrease. The average signal during room air ventilation remained relatively unchanged.

The amplitude of the activation-induced signal change was damped during the period of increased CO_2 ventilation, yet the overall signal increased. The absolute peak activation amplitude is higher during hypercapnia. The amplitude of the activation-induced signal change was only slightly damped during the period of decreased oxygen ventilation, possibly indicating that

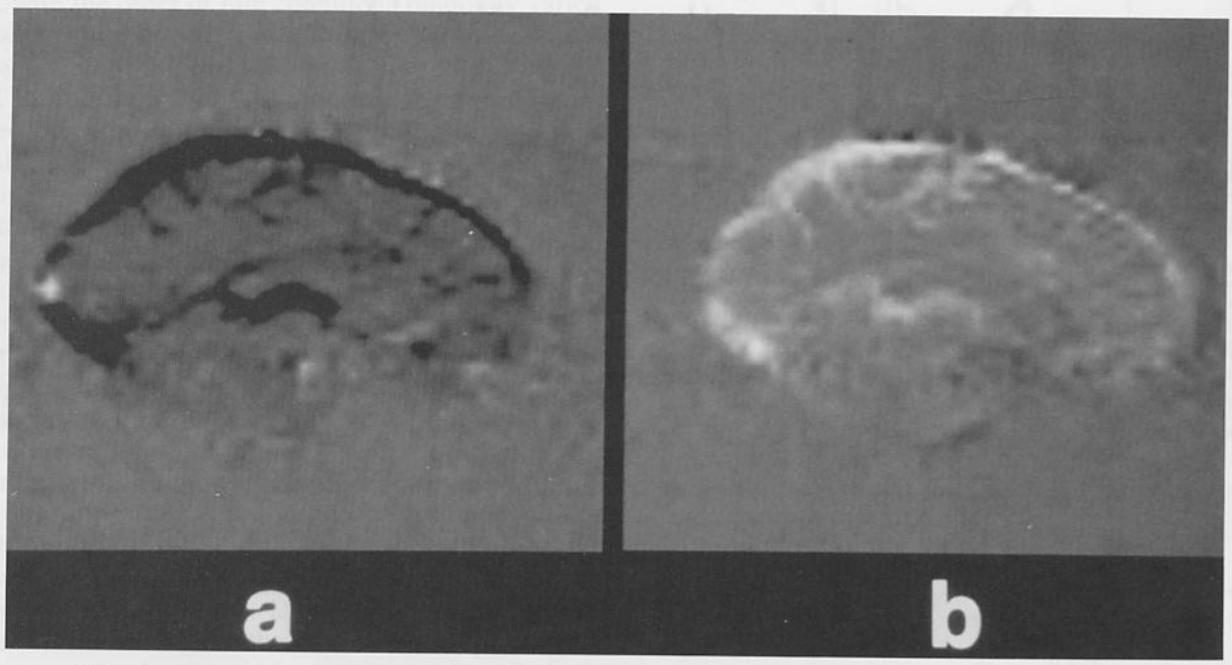

FIG. 10. Images created by subtraction, in each time course, of the average of 10 images obtained during baseline from 40 images obtained during **(a)** inspired 12% O_2 (hypoxia) and **(b)** inspired 5% CO_2 (hypercapnia). The regions which appear to have highest blood volume show the largest signal decreases during hypoxia and the largest signal increase during hypercapnia. Hypoxia is understood to decrease arterial and venous oxygenation, thus decreasing the signal. Hypercapnia is known to increase blood flow without an increase in metabolic rate, thus causing an increase in primarily the venous oxygenation.

the mechanism that increases flow during activation is not significantly affected by decreased oxygenation. In addition, the evidence suggests either that a feedback mechanism for supplying an adequate oxygen supply during activation is either not strong or nonexistent, since activation induced signal changes are readily modulated above and below normal states.

Time courses of images obtained from a resting brain during the same three experiments as mentioned above were used to map the relative signal changes on a pixel by pixel basis. Figure 9 illustrates an echo-planar image of the slice observed. Figure 10a is an image that was created by subtraction of the average of images during the baseline period from the average of images obtained during the hypoxic state. Regions that appear to have high blood volume have the largest signal changes. Figure 10b is an image that was created by subtraction of images during the baseline period from the average of images obtained during the hypercapnic state. Again, regions of high blood volume show the most pronounced changes. In the case of hypoxia, a negative change takes place. In the case of hypercapnia, a positive change takes place. Given an oxygenation change that is homogeneously distributed throughout the vasculature, the magnitude of signal change would be roughly proportional to the blood volume in a given pixel. In such a manner, maps of blood volume may be made noninvasively.

If effects on arterial and venous blood oxygenation can be quantitatively correlated with changes in the content of inspired gases, the potential exists for accurately localizing and quantitatively correlating activation-induced signal changes with specific hemodynamic changes associated with underlying neuronal activation. In other words, if the effects of alterations in inspired gases on various hemodynamic factors are well characterized using other methods, then the activation-induced MR signal changes would be better understood and potentially quantifiable in an absolute manner.

In addition, the technique of using well characterized perturbations of blood oxygenation as probes in conjunction with a combined gradient-echo and spin-echo EPI sequence (21) may allow the determination of the pixel by pixel distribution of blood volume and vessel radii in active and resting brain regions. Such information would also prove to be a valuable correlate to biophysical models of BOLD contrast in the brain.

DATA ANALYSIS TECHNIQUES

Use of Dynamic Characteristics for the Creation of Brain Activity Images

The use of a time course of rapidly obtained images of the same plane in combination with control of brain activation timing results in data that may be processed in several different ways. The principle driving the development of the techniques is that the dynamics of the activation-induced signal changes provide unique information which allows for robust differentiation from artifactual signal changes.

Time course data may be analyzed in the temporal domain, or, after Fourier transformation, the frequency domain.

In the time domain, images highlighting regions of activation and their relative magnitudes of activation can be created by calculation of the scalar product of a vector representing the expected temporal response with the response of every pixel. With this technique, the entire time course is used, including those images that are in transition between the "resting" and "active" states. This technique has been shown to be a sensitive and robust means of extracting functional information from temporal data sequences, but requires user input in the choice of the reference vector. A reference vector may be obtained by (i) choosing the pixel containing what appears to be the "best" temporal response, (ii) averaging in time the activation cycles in a "best temporal response" pixel then duplicating the time-averaged cycle for the length of the time course, (iii) averaging in space several of the "best temporal response" pixels, (iv) synthesizing a reference vector, or (v) choosing a vector obtained from principal component analysis of the time course.

In the Fourier domain, if the activation paradigm is periodic, then a specific spectral density image, at the activation frequency, will show high signal intensity in periodically changing regions of the brain. If spectral density images are observed, only the rate of activation need be known to create a brain activation image.

The techniques described above still fall short of differentiating many of the artifactual from activation-induced signal changes. Much of the artifactual signal enhancement that occurs in time is a result of very large signal changes that are spuriously correlated with the activation paradigm timing and have broad-band frequency content. Such changes occur in regions of pulsatile blood or csf flow or pulsatile brain motion. A method for removing these artifacts revolves around the central idea of calculating, on a pixel-by-pixel basis, the *correlation coefficient*, as opposed to the correlation, of a reference vector representing the expected temporal response from activated regions of the brain with the time response of every pixel in the image (37). The calculated correlation coefficients are dependent upon the relative shapes of the time responses and not on the relative magnitudes. A threshold correlation coefficient may then be chosen to eliminate all signal changes that do not have sufficient shape correlation with the reference function. If the assumption is made that the noise has a gaussian variance around the refer-

ence vector, the statistical significance, p, is uniquely related to the correlation coefficient, r, and the degrees of freedom of images in the time course, N, by:

$$p = 1 - \frac{2}{\sqrt{\pi}} \int_0^{|r|\sqrt{N/2}} e^{-t^2}\, dt.$$

After thresholding, the scalar product, or correlation, is calculated using those pixels that have survived the shape thresholding, so that relative magnitude information is present in the functional images. Artifacts from spurious correlations that would have appeared in simple subtraction images, direct scalar product images, or spectral density images are effectively removed in this manner. The correlation coefficient calculations may also be performed in the frequency domain, which may be particularly useful if "activated" brain regions have complicated spectra which are different from "resting" brain spectra. Such may be the case in regions of higher cognitive processing which may be "active" at various times during a desired "resting" period, so that a proper baseline could never be established. Instead of relying upon signal changes correlated with discrete activation changes, one may observe changes in activation rates by analysis of data in the Fourier domain. Regions such as the hippocampus, which may never be discretely "off" or "on," but may change state in some manner, might lend themselves to such an analysis technique.

The techniques described above are demonstrated in the following example. A time course of 128 axial images containing the left and right motor cortices (TR = 2 s) was obtained in which the task was interleaved, alternate-hand self-paced tapping of fingers to thumb. The subject was instructed to tap the right fingers for eight images (16 s) and then immediately tap the left fingers for 16 s, and so on, until the end of the time course. Figure 11 displays the first image in the time course with boxed regions over the right (a) and left (b) motor cortices as well as a box over the sagittal sinus region (c). Figure 12A–C are 7 × 7 pixel time course displays corresponding to the boxed regions of Fig. 11. A reference vector, obtained by averaging in time the activation cycles in a "best temporal response" pixel in the left motor cortex, then duplicating the time-averaged cycle for the length of the time course, is shown in Figure 13. The scalar product of the reference vector with the time course of every pixel was performed. The result is illustrated in Figure 14. Note that while the regions in the motor cortices show signal enhancement (opposite sign because the left/right activation was exactly 180° out of phase), the sagittal sinus region, having large but randomly correlated signal changes, shows enhancement as well. To remove the large, randomly correlated artifacts, the correlation coefficient (i.e., scalar product calculation after time-course normalization) is calculated for the time course of each pixel. Figure 15 illustrates a correlation coefficient image obtained with the same data set and reference vector. Note the difference between the correlation coefficient image and Figure 14. The sagittal sinus shows minimal correlation, and therefore much reduced signal intensity in Figure 15. Finally, by choosing a 0.5 correlation coefficient threshold for scalar production calculation, all pulsatile artifacts are removed. Figure 16 *(see Color Plate 16 in color section)* shows the functional image (superimposed upon the first image in the time course series) obtained using such a threshold. Positive and negative correlations are shown in red and blue respectively.

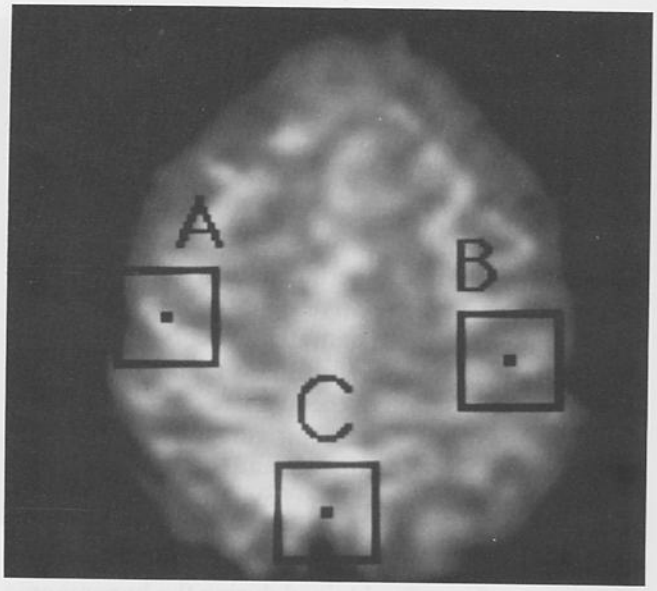

FIG. 11. Axial image containing the motor cortices (TE/TR = 40 ms/∞). This is the first image from the echo-planar time course series and is used as an anatomical reference. Boxes A, B, and C are 7 × 7 pixel regions which presumably cover the right and left motor cortices, and the sagittal sinus, respectively. The time-course displays, shown in Figure 12A–C, are from the boxed regions.

Conversion of the time course of images into spectral density images allows one to localize the periodically changing signal simply by observation of the spectral density image at the specific frequency of activation. In this case, the image at 0.031 Hz (the on/off activation frequency) is shown in Figure 17. Note that the sagittal sinus shows enhancement due to the broad-band spectral content pulsatile flow artifact. Such an artifact may be eliminated by correlation coefficient calculation of a reference spectrum with the frequency response of every pixel. Calculation of the correlation coefficient in the frequency domain is useful for finding spectra which do not have a single peak but a unique pattern of spectral peaks associated with an activated state.

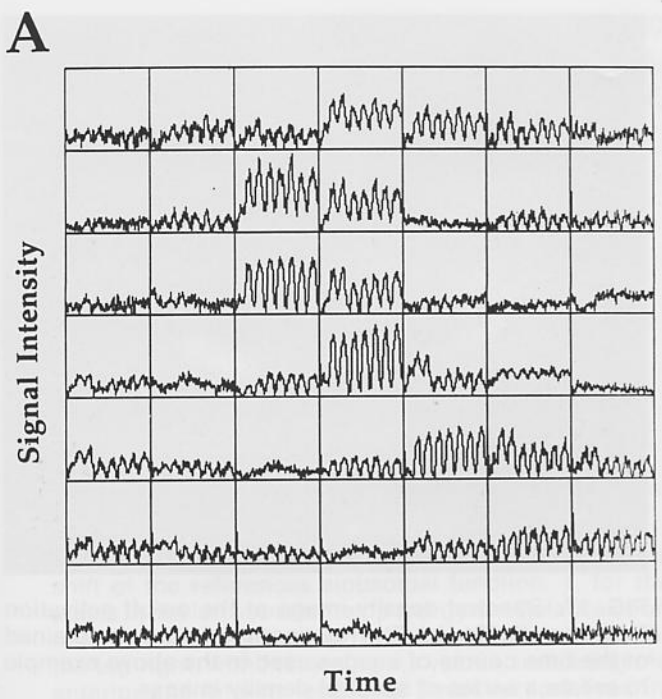

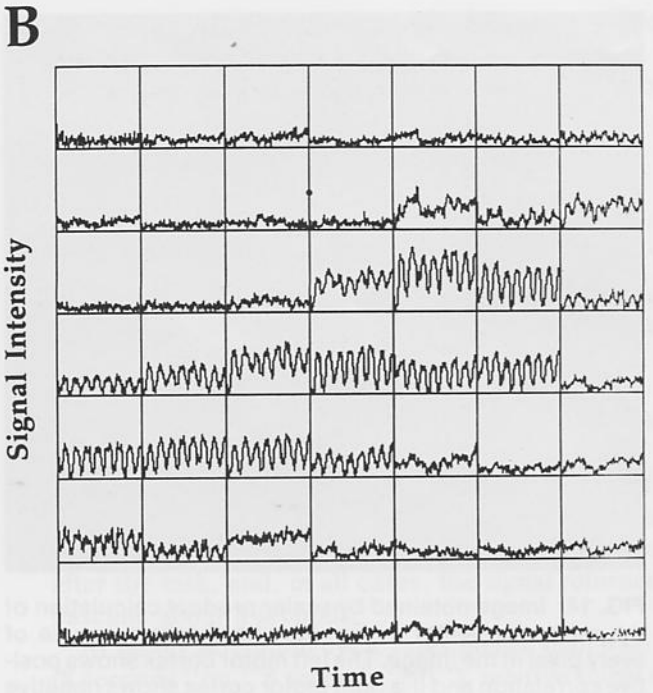

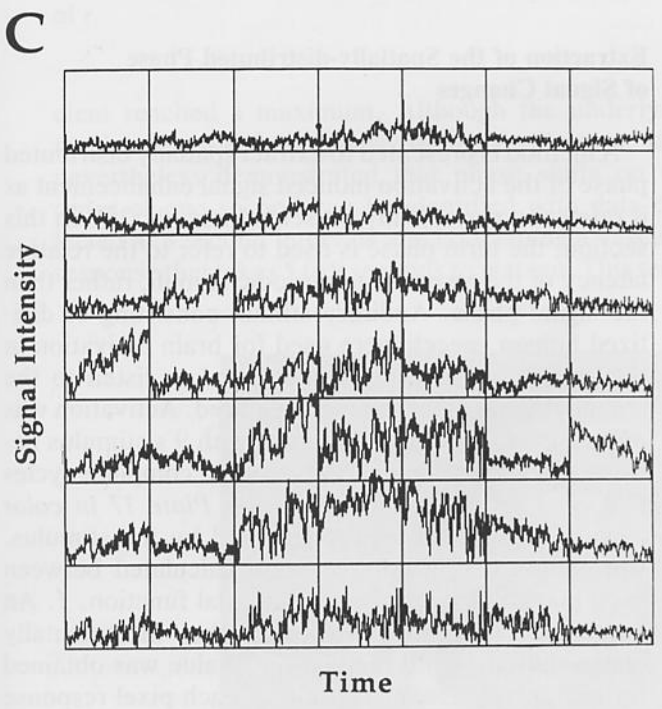

FIG. 12. Time-course displays from the boxed regions in Fig. 11 (TE/TR = 40 ms/2,000 ms). The time course consisted of 128 images, during which the subject tapped the right fingers for 16 s then immediately switched to tapping of the left fingers without pause, and so on. **A, B:** Active regions, revealed by the signal changes temporally correlated to the activation time course, are sharply outlined. Signal changes in the sagittal sinus **(C)** are most likely due to time-of-flight pulsatile flow effects. Signal changes are large and spuriously correlated to the activation paradigm of either hand. The relative scales of all plots are the same.

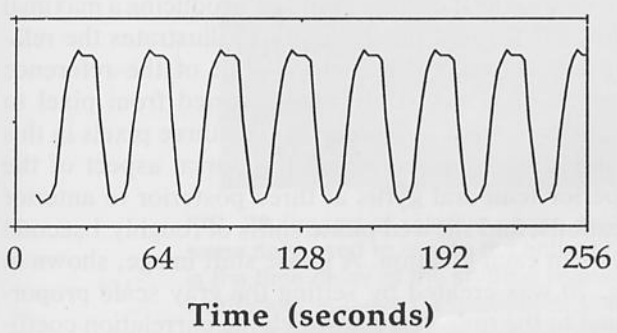

FIG. 13. Reference vector used for creation of images shown in Figs. 14–16. The vector was created by averaging in time the activation cycles in a "best temporal response" pixel in the left motor cortex, then duplicating the time-averaged cycle for the length of the time course.

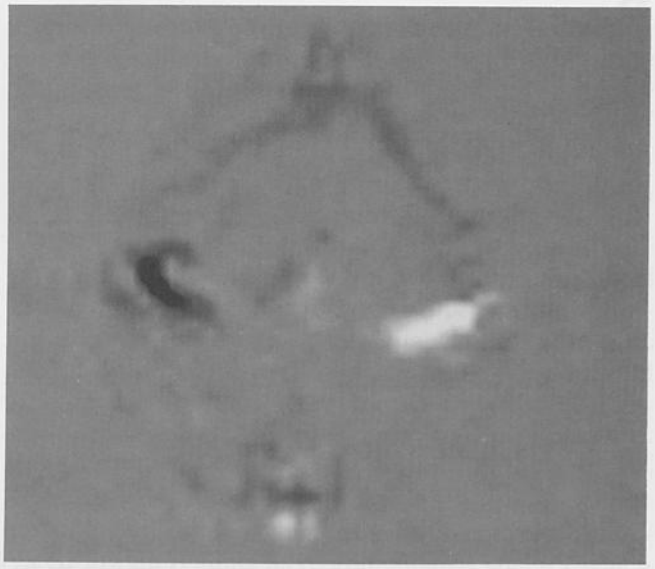

FIG. 14. Image obtained by scalar product calculation of the reference vector in Fig. 13 with the time course of every pixel in the image. The left motor cortex shows positive correlation and the right motor cortex shows negative correlation due to the fact that the finger activation timing was exactly 180° out of phase between hands. The sagittal sinus region show high signal intensity, yet Fig. 12C demonstrates that the time response is, at best, spuriously correlated with the activation time course.

FIG. 15. Image obtained by calculation of the correlation coefficient with the reference vector in Fig. 15. Note that the sagittal sinus has a small temporal correlation coefficient with the reference vector, but has a high signal intensity in the scalar product image.

FIG. 17. Spectral density image at the on/off activation frequency (0.031 Hz). The Fourier transform was obtained of the time course of images used in the above example to create a series of spectral density images.

Extraction of the Spatially-distributed Phase of Signal Changes

A method is presented to extract spatially distributed phase of the activation induced signal enhancement as it relates to periodically presented stimuli (38). In this section, the term phase is used to refer to the relative latency of the response to periodic stimuli, rather than the signal phase. Auditory stimuli consisting of digitized human speech were used for brain activation in this study. Subjects were instructed to listen to the stimuli, but no other task was required. Activation was performed in a periodic manner, with 9 s stimulus periods and 9 s baseline periods over 10 complete cycles (TR = 3 s). Figure 18 *(see Color Plate 17 in color section)* shows the region activated by the stimulus. Correlation coefficients, r, were calculated between each pixel and a reference sinusoidal function, f. An automated procedure was used that incrementally phase-shifted f until the highest r value was obtained for each pixel. The phase shift of each pixel response was defined as the phase shift of f producing a maximal value of r for that pixel. Figure 19 illustrates the relationship between r and phase shift of the reference function, f. Phase shift values varied from pixel to pixel by as much as 3 seconds. The three pixels in this example were spaced along the dorsal aspect of the superior temporal gyrus at three posterior to anterior locations, and showed phase shifts of roughly 1 second between each location. A phase shift image, shown in Fig. 20 was created by setting the gray scale proportional to the time delay at which the correlation coeffi-

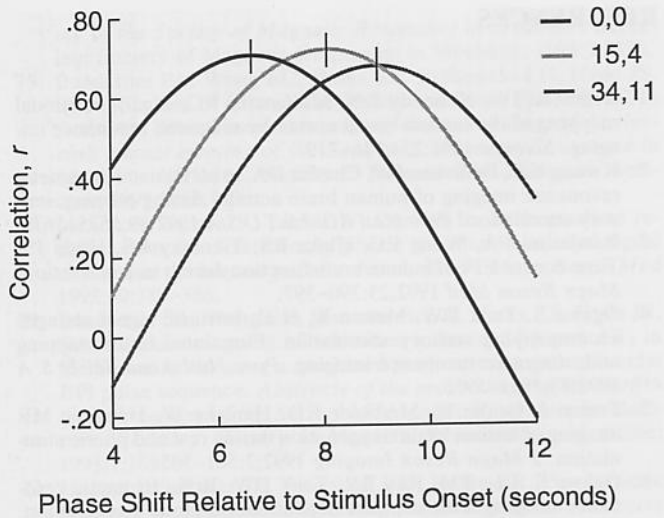

FIG. 19. Correlation coefficient, *r*, as a function of phase shift of the references sinusoidal function, *f*, for three pixels in the left superior temporal gyrus. Relative coordinate locations, in mm, of the three pixels are given at the top right, with increasing *x,y* values, indicating more anterior and inferior locations. Small vertical lines indicate the phase shift of *f* resulting in a maximal value of *r*.

cient reached a maximum. Although the underlying mechanism for these phase shifts is unknown, it is nevertheless demonstrated that phase shifts on the order of one second can be identified with data collected at 3 second intervals and concerning a vascular response that takes 5 to 9 seconds to plateau. This technique would be particularly applicable to the temporal analysis of behaviors characterized by extended, sequential activity, as in cognitive tasks that involve widely distributed neural networks.

CONCLUSIONS

One goal of these studies was to obtain a better understanding of the response characteristics of the activation-induced BOLD signal change. With the use of T_2^*-weighted EPI, time courses of sequentially obtained images of the brain were collected. During the time courses, primary motor and auditory tasks were varied in duration, timing, and rate.

During extended activation durations, the signal remained elevated. During activations as brief as 0.5 seconds, a signal increase was detected about 3 seconds after the task, and, in all cases, the signal returned to baseline about 8 seconds.

At on/off activation cycle rates higher than 0.06 Hz (8 seconds "on," 8 seconds "off"), relative signal amplitude was damped, and, at rates higher than 0.13 Hz (4 seconds "on," 4 seconds "off"), the hemodynamic response did not follow the activation timing.

Signal change in the motor and auditory cortices was stimulus rate dependent. In the range of activation rates studied (motor: 1 Hz to 5 Hz, auditory: 0.17 Hz to 2.5 Hz), the percent signal change increased in a monotonic manner with rate.

The activation-induced signal change in the motor cortex was observed in the presence of alterations in

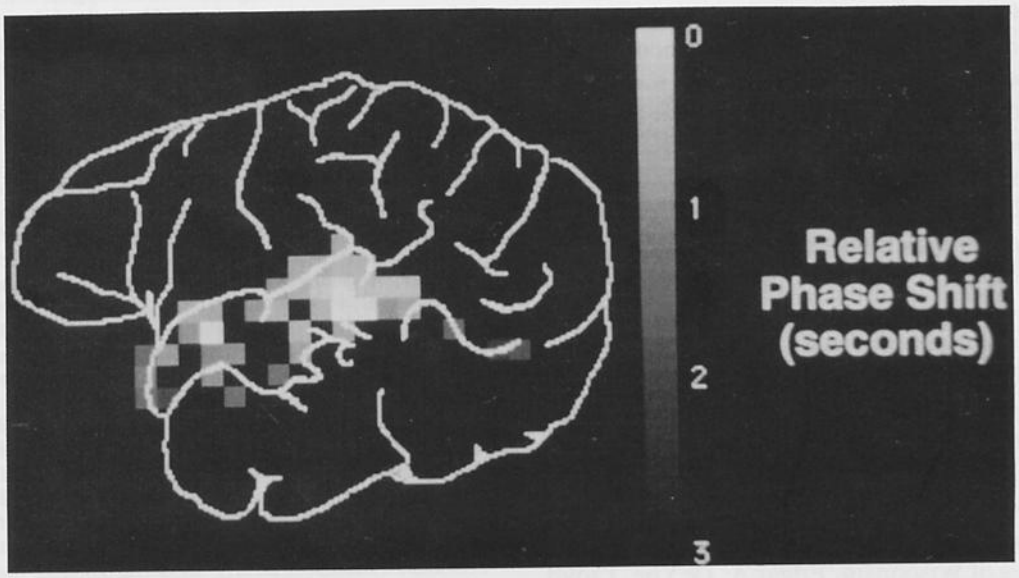

FIG. 20. Image of relative phase shift of the activation-induced signal enhancement from the same data used to create the activation images shown in Fig. 18 *(Color Plate 17)*. The gray scale is the time delay of the shifting reference sinusoidal function, per pixel, at which the correlation coefficient achieved a maximum. The phase of the maximal correlation coefficient appears to move in the anterior and inferior directions along the superior temporal gyrus.

the concentrations of inspired CO_2 and O_2. With inspired CO_2 (5%), the overall signal increased roughly in proportion to blood volume in each pixel, and the activation-induced signal change was strongly damped. With a decrease in inspired O_2 (21% to 12%), the overall signal decreased roughly in proportion to blood volume in each pixel, and the activation-induced signal change was not significantly damped.

The technique of mapping brain function based on BOLD contrast in MRI fills a large spatial and temporal niche among the currently available brain function imaging modalities (50). In addition, in no other technique is it possible to obtain data which is intrinsically registered with anatomical MR images.

These studies also included an overview of some methods that are able to be applied to time course series of susceptibility-weighted images to create brain activation images which have reduced artifactual contamination. The use of a time course of images in conjunction with control over activation timing and an understanding of the dynamics of the activation-induced signal changes allow for application of post-processing methods which include temporal cross correlation and Fourier analysis. Such techniques allow differentiation activation-induced signal changes from artifactual signal changes. In addition, differences in signal change latency on the order of one second may be differentiated by time shifting the temporal reference function.

Activation-induced BOLD signal changes arising from higher order cognitive function may not be as well behaved, as large, or as consistent as those arising from the primary sensory and motor cortices. The application of neuro-functional MRI to understanding of higher cognitive function will require sophisticated activation time course planning and post-processing in conjunction with a solid understanding of the nature of the artifactual signal changes.

As our understanding of the dynamics of BOLD contrast and, more generally, the dynamics of brain function grows, activation paradigm and post-processing methods will evolve so that more subtle information about brain function and physiology may be obtained.

ACKNOWLEDGMENTS

This work was supported, in part, by grants CA41464 and RR01008 from the National Institutes of Health. P.A.B. thanks GE Medical Systems for financial support. In addition, the support of our colleagues at the Medical College of Wisconsin, Edgar A. DeYoe, Lloyd D. Estkowski, Thomas A. Hammeke, Michael D. Goldstein, Victor M. Haughton, George L. Morris, Wade M. Meuller, Joel B. Myklebust, F. Zerrin Yetkin, and Jeffrey R. Zigun, is gratefully appreciated.

REFERENCES

1. Belliveau JW, Kennedy DN, McKinstry RC, et al. Functional mapping of the human visual cortex by magnetic resonance imaging. *Science* 1991;254:716–719.
2. Kwong KK, Belliveau JW, Chesler DA, et al. Dynamic magnetic resonance imaging of human brain activity during primary sensory stimulation. *Proc Natl Acad Sci U S A* 1992;89:5675–5679.
3. Bandettini PA, Wong EC, Hinks RS, Tikofsky RS, Hyde JS. Time course EPI of human brain function during task activation. *Magn Reson Med* 1992;25:390–397.
4. Ogawa S, Tank DW, Menon R, et al. Intrinsic signal changes accompanying sensory stimulation: Functional brain mapping with magnetic resonance imaging. *Proc Natl Acad Sci U S A* 1992;89:5951–5955.
5. Frahm J, Bruhn H, Merboldt KD, Hanicke W. Dynamic MR imaging of human brain oxygenation during rest and photic stimulation. *J Magn Reson Imaging* 1992;2:501–505.
6. Ogawa S, Lee TM, Kay AR, Tank DW. Brain magnetic resonance imaging with contrast dependent on blood oxygenation. *Proc Natl Acad Sci U S A* 1990;87:9868–9872.
7. Cooper R, Papakostopoulos D, Crow HJ. Rapid changes of cortical oxygen associated with motor and cognitive function in man. *Blood flow and metabolism in the brain*. Aviermore, Scotland: Churchill Livingstone, 1975;1:14.8–14.9.
8. Fox PT, Raichle ME. Focal physiological uncoupling of cerebral blood flow and oxidative metabolism during somatosensory stimulation in human subjects. *Proc Natl Acad Sci U S A* 1986; 83:1140–1144.
9. Frostig RD, Lieke EE, Ts'o DY, Grinvald A. Cortical functional architecture and local coupling between neuronal activity and the microcirculation revealed by *in vivo* high-resolution optical imaging of intrinsic signals. *Proc Natl Acad Sci U S A* 1990;87: 6082–6086.
10. Villringer A, Planck J, Hock C, Schleinkofer L, Dirnagl U. Near infrared spectroscopy (NIRS): A new tool to study hemodynamic changes during activation of brain function in human adults. *Neurosci Lett* 1993;154:101–104.
11. Turner R, LeBihan D, Moonen CT, Despres D, Frank J. Echo-planar time course MRI of cat brain oxygenation changes. *Magn Reson Med* 1991;22:159–166.
12. Hoppel BE, Weisskoff RM, Thulborn KR, Moore J, Rosen BR. Measurement of regional brain oxygenation state using echo planar linewidth mapping. *Abstracts of the proceedings of the tenth annual meeting of the Society of Magnetic Resonance in Medicine*. Berkeley: Society of Magnetic Resonance in Medicine; 1991;1:308.
13. Stehling MK, Schmitt F, Ladebeck R. Echo-planar MR imaging of human brain oxygenation changes. *J Magn Reson Imaging* 1993;3:471–474.
14. De Crespigny AJ, Tsuura M, Moseley ME. Real time detection of blood oxygenation changes during apnea in partially ischemic rat brain at 4.7 T. *Abstracts of the proceedings of the tenth annual meeting of the Society of Magnetic Resonance in Medicine*. Berkeley: Society of Magnetic Resonance in Medicine; 1992;1:914.
15. Jezzard P, Heineman F, Taylor J, Despres D, Wen H, Turner R. Comparisons of EPI gradient-echo contrast changes in cat brain caused by respiratory challenges with direct spectrophotometric evaluation of cerebral oxygenation via a cranial window. *Abstracts of the proceedings of the tenth annual meeting of the Society of Magnetic Resonance in Medicine*. Berkeley: Society of Magnetic Resonance in Medicine; 1992;1:918.
16. Turner R, Jezzard P, Wen H, Kwong KK, LeBihan D, Zeffiro T, Balaban RS. Functional mapping of the human visual cortex at 4 and 1.5 Tesla using deoxygenation contrast EPI. *Magn Reson Med* 1993;29:277–279.
17. Frahm J, Merboldt KD, Hänicke W, Functional MRI of human brain activation at high spatial resolution. *Magn Reson Med* 1993;29:139–144.
18. Jesmanowicz A, Bandettini PA, Wong EC, Tan G, Hyde JS. Spin-echo and gradient-echo EPI of human brain function at 3 Tesla. *Abstracts of the proceedings of the twelfth annual meet-*

ing of the Society of Magnetic Resonance in Medicine. Berkeley: Society of Magnetic Resonance in Medicine; 1993;3:1390.
19. Bandettini PA, Wong EC, Hinks RS, Estkowski LD, Hyde JS. Quantification of Changes in Relaxation Rates R2* and R2 in Activated Brain Tissue. *Abstracts of the proceedings of the eleventh annual meeting of the Society of Magnetic Resonance in Medicine*. Berkeley: Society of Magnetic Resonance in Medicine; 1992;WIP:719.
20. Menon R, Ogawa S, Tank DW, Ugurbil K. Tesla gradient recalled echo characteristics of photic stimulation-induced signal changes in the human primary visual cortex. *Magn Reson Med* 1993;30:380–386.
21. Bandettini PA, Wong EC, Jesmanowicz A, Hinks RS, Hyde JS. Simultaneous mapping of activation-induced ΔR_2^* and ΔR_2 in the human brain using a combined gradient-echo and spin-echo EPI pulse sequence. *Abstracts of the proceedings of the twelfth annual meeting of the Society of Magnetic Resonance in Medicine*. Berkeley: Society of Magnetic Resonance in Medicine; 1993;1:169.
22. Hoppel BE, Baker JR, Weisskoff RM, Rosen BR. The dynamic response of ΔR2 and ΔR2′ during photic activation. *Abstracts of the proceedings of the twelfth annual meeting of the Society of Magnetic Resonance in Medicine*. Berkeley: Society of Magnetic Resonance in Medicine; 1993;3:1384.
23. Kwong KK, Chesler DA, Zuo CS, et al. Spin-echo (T2, T1) studies for functional MRI. *Abstracts of the proceedings of the twelfth annual meeting of the Society of Magnetic Resonance in Medicine*. Berkeley: Society of Magnetic Resonance in Medicine; 1993;1:172.
24. Turner R, Jezzard P, Le Bihan D, Prinster A. Contrast mechanisms and vessel size effects in BOLD contrast functional neuroimaging. *Abstracts of the proceedings of the twelfth annual meeting of the Society of Magnetic Resonance in Medicine*. Berkeley: Society of Magnetic Resonance in Medicine; 1993;1:173.
25. Weisskoff RM, Hoppel BJ, Rosen BR. Signal changes in dynamic contrast studies: Theory and experiment *in vivo*. *J Magn Reson Imaging* 1992;2P:77.
26. Ogawa S, Menon RS, Tank DW, Kim S-G, Merkle H, Ellermann JM, Ugŭrbil K. Functional brain mapping by blood oxygenation level-dependent contrast magnetic resonance imaging. A comparison of signal characteristics with a biophysical model. *Biophys J* 1993;64(3):803–812.
27. Boxerman JL, Weisskoff RM, Hoppel BE, Rosen BR. MR contrast due to microscopically heterogeneous magnetic susceptibility: cylindrical geometry. *Abstracts of the proceedings of the twelfth annual meeting of the Society of Magnetic Resonance in Medicine*. Berkeley: Society of Magnetic Resonance in Medicine; 1993;1:389.
28. Wong EC, Bandettini PA. A deterministic method for computer modelling of diffusion effects in MRI with application to BOLD contrast imaging. *Abstracts of the proceedings of the twelfth annual meeting of the Society of Magnetic Resonance in Medicine*. Berkeley: Society of Magnetic Resonance in Medicine; 1993;1:10.
29. DeYoe EA, Neitz J, Bandettini PA, Wong EC, Hyde JS. Time course of event-related MR signal enhancement in visual and motor cortex. *Abstracts of the proceedings of the eleventh annual meeting of the Society of Magnetic Resonance in Medicine*. Berkeley: Society of Magnetic Resonance in Medicine; 1992; WIP:1824.
30. Blamire AM, Ogawa S, Ugŭrbil K, et al. Dynamic mapping of the human visual cortex by high speed magnetic resonance imaging. *Proc Natl Acad Sci U S A* 1992;89:11069–11073.
31. Binder JR, Rao SM, Hammeke TA, et al. Temporal characteristics of functional magnetic resonance signal change in lateral frontal and auditory cortex. *Abstracts of the proceedings of the twelfth annual meeting of the Society of Magnetic Resonance in Medicine*. Berkeley: Society of Magnetic Resonance in Medicine; 1993:5.
32. Menon RS, Ogawa S, Kim S-G, Ellerman JM, Merkle H, Tank DW, Ugŭrbil K. Functional brain mapping using magnetic resonance imaging: Signal changes accompanying visual stimulation. *Invest Radiol* 1992;27:S47–S53.
33. Fox PT, Raichle ME. Stimulus rate dependence of regional cerebral blood flow in human striate cortex, demonstrated by positron emission tomography. *J Neurophysiol* 1984;51:1109–1120.
34. Frahm J, Merboldt KD, Hänicke W. Tissue vs. vascular effects and changes of flow vs. deoxyhemoglobin? Problems revealed by functional brain imaging at high spatial resolution. *Abstracts of the proceedings of the twelfth annual meeting of the Society of Magnetic Resonance in Medicine*. Berkeley: Society of Magnetic Resonance in Medicine; 1993;3:1427.
35. Lai S, Hopkins AL, Haacke EM, et al. Identification of vascular structures as a major source of signal contrast in high resolution 2D and 3D functional activation imaging of the motor cortex at 1.5 T: Preliminary results. *Magn Reson Med* 1993;30:387–392.
36. Mansfield P. Multi-planar image formation using NMR spin echoes. *J Phys* 1977;C10:L55–L58.
37. Bandettini PA, Jesmanowicz A, Wong EC, Hyde JS. Processing strategies for time-course data sets in functional MRI of the human brain. *Magn Reson Med* 1993;30:161–173.
38. Binder JR, Jesmanowicz A, Rao SM, Bandettini PA, Hammeke TA, Hyde JS. Analysis of phase differences in periodic functional MRI activation data. *Abstracts of the proceedings of the twelfth annual meeting of the Society of Magnetic Resonance in Medicine*. Berkeley: Society of Magnetic Resonance in Medicine; 1993;3:1383.
39. Wong EC, Bandettini PA, Hyde JS. Echo-planar imaging of the human brain using a three axis local gradient coil. *Abstracts of the proceedings of the eleventh annual meeting of the Society of Magnetic Resonance in Medicine*. Berkeley: Society of Magnetic Resonance in Medicine; 1992;1:105.
40. Wong EC, Boskamp E, Hyde JS. A volume optimized quadrature elliptical endcap birdcage brain coil. *Abstracts of the proceedings of the eleventh annual meeting of the Society of Magnetic Resonance in Medicine*. Berkeley: Society of Magnetic Resonance in Medicine; 1992;2:4015.
41. Fox PT, Raichle ME. Stimulus rate determines regional brain blood flow in striate cortex. *Ann Neurol* 1985;17:303–305.
42. Price C, Wise R, Ramsay S, et al. Regional response differences within the human auditory cortex when listening to words. *Neurosci Lett* 1992;146:179–182.
43. Binder JR, Rao SM, Hammeke TA, et al. Effects of stimulus rate on signal response during functional magnetic resonance imaging of auditory cortex. *Cognitive Brain Research* 1994;2: 31–38.
44. Pratt H, Sohmer H. Intensity and rate function in cochlear and brainstem evoked responses to click stimuli in the man. *Arch Otorhinolaryngol Head Neck Surgery* 1976;212:85–92.
45. Suzuki T, Kobayashi K, Takagi N. Effects of stimulus repetition rate on slow and fast components of auditory brain-stem responses. *Electroencephalogr Clin Neurophysiol* 1970;28: 360–367.
46. Vaughn HG, Ritter W. The sources of auditory evoked responses recorded from the human scalp. *Electroencephalogr Clin Neurophysiol* 1970;28:360–367.
47. Wood CC, Wolpaw JR. Scalp distribution of human evoked potentials: II. Evidence for overlapping sources and involvement of auditory cortex. *Electroencephalogr Clin Neurophysiol* 1982; 54:25–38.
48. Davis H, Mast T, Yoshie N, et al. The slow response of the human cortex to auditory stimuli: Recovery process. *Electroencephalogr Clin Neurophysiol* 1966;21:105–113.
49. Nelson DA, Lassman FM. Effects of intersignal interval on the human auditory evoked response. *J Acoust Soc Am* 1968;44: 1529–1532.
50. Belliveau JW, Kwong KK, Kennedy DN, et al. Magnetic resonance imaging mapping of brain function: Human visual cortex. *Invest Radiol* 1992;27:S59–S65.

Also apparent is some gray-white matter contrast. **B.** An over

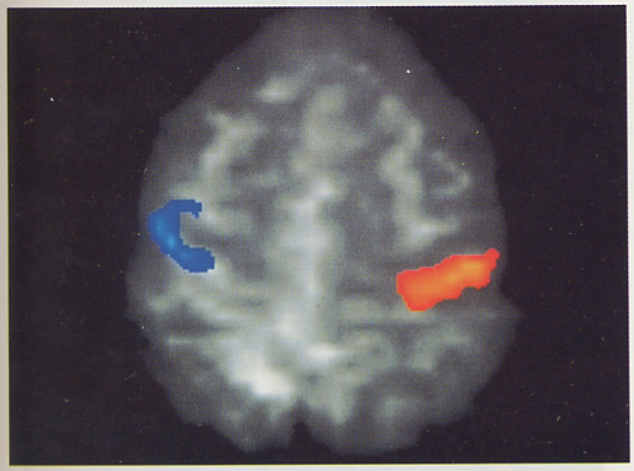

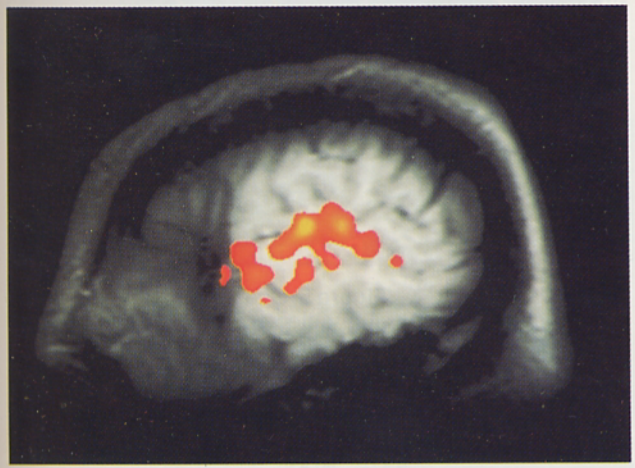

COLOR PLATE 17. (Figure 18, Chapter 18) Brain activation image showing signal enhancement in the left superior temporal gyrus as a result of human speech stimuli.

◀ **COLOR PLATE 16.** (Figure 16, Chapter 18) After all pixels which had a correlation coefficient less than 0.5 ($p < 1.5 \times 10^{-8}$) were removed, the correlation was calculated on the remaining pixels so that relative magnitude information would be placed back into the functional image. Positive correlation is shown in red and negative correlation is in blue.

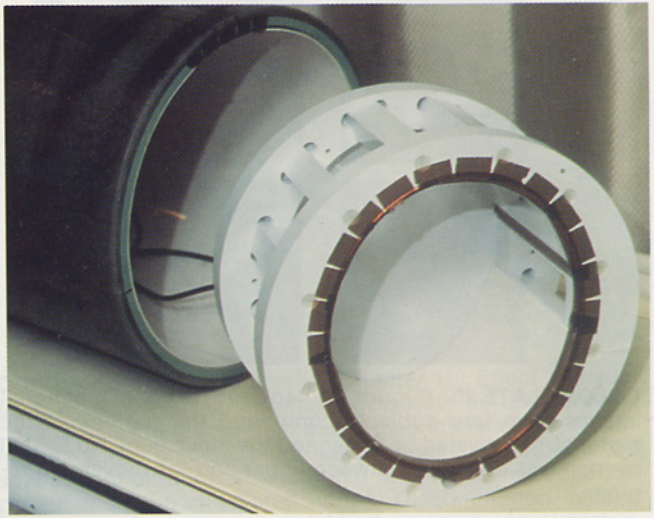

COLOR PLATE 18. (Figure 1, Chapter 19) The three-axis gradient coil and quadrature radiofrequency coil setup shown allows for the performance of entire brain neurofunctional MRI using single-shot echo-planar imaging on an otherwise standard clinical scanner.